SCIENTIFIC REPORTS

OPEN

SUBJECT AREAS:
STRUCTURAL PROPERTIES
MECHANICAL PROPERTIES

Received
25 October 2013

Accepted
6 December 2013

Published
8 January 2014

Correspondence and requests for materials should be addressed to G.L. (lgsammer@mail.xjtu.edu.cn) or J.S. (junsun@mail.xjtu.edu.cn)

Microalloying Ultrafine Grained Al Alloys with Enhanced Ductility

L. Jiang[1], J. K. Li[1], P. M. Cheng[1], G. Liu[1], R. H. Wang[2], B. A. Chen[1], J. Y. Zhang[1], J. Sun[1], M. X. Yang[3] & G. Yang[3]

[1]State Key Laboratory for Mechanical Behavior of Materials, Xi'an Jiaotong University, Xi'an, 710049, PR China, [2]School of Materials Science and Engineering, Xi'an University of Technology, Xi'an, 710048, PR China, [3]Central Iron and Steel Research Institute, Beijing, 100081, PR China.

Bulk ultrafine grained (UFG)/nanocrystal metals possess exceptional strength but normally poor ductility and thermal stability, which hinder their practical applications especially in high-temperature environments. Through microalloying strategy that enables the control of grains and precipitations in nanostructured regime, here we design and successfully produce a highly microstructure-stable UFG Al-Cu-Sc alloy with ~275% increment in ductility and simultaneously ~50% enhancement in yield strength compared with its Sc-free counterpart. Although the precipitations in UFG alloys are usually preferentially occurred at grain boundaries even at room temperature, minor Sc addition into the UFG Al-Cu alloys is found to effectively stabilize the as-processed microstructure, strongly suppress the θ-Al_2Cu phase precipitation at grain boundary, and remarkably promote the θ'-Al_2Cu nanoparticles dispersed in the grain interior in artificial aging. A similar microalloying strategy is expected to be equally effective for other UFG heat-treatable alloys.

Ultrafine grained (UFG) Al alloys have attracted growing attention owing to their strikingly improved strength[1–4]. However, they usually have disappointingly low ductility at ambient temperatures due to insufficient dislocation accumulation capability[5–8], which limits the practical applications of UFG alloys. Some strategies have been proposed[1–9] to improve tensile ductility of the UFG alloys. In particular, dispersing nanosized particles in the grain interior has been considered[5,8,9] as the simplest but best approach applicable for the UFG Al alloys. The reason is that nanosized particles could be naturally precipitated within the grains through aging treatment, as industrially applied in coarse grained (CG) Al alloys[10,11]. However, intragranular precipitation in the UFG Al alloys will be heavily hindered. The UFG alloys produced by severe plastic deformation are characterized by "non-equilibrium" high angle grain boundaries (GBs), which will preferentially motivate intergranular precipitation even at room temperature[12]. The intergranular hard particles introduce stress concentration at the grain boundaries and tend to localize strain and cracking near them, resulting in intergranular fracture and unresolved low ductility[13]. In the UFG Al alloys produced by using equal-channel angular pressing (ECAP), some studies[14–17] have reported on adjusting the post-ECAP aging process (i.e., choosing an appropriate time-temperature-regime for aging after a low number of ECAP-passes) to achieve suitable combinations of strength and ductility. However, the precipitation behaviors in UFG Al alloys are still far from controllable and reproducible, which restricts the development of advanced UFG Al alloys with tailored nanoparticle distribution and high ductility.

The key to prolong ductility of UFG Al alloys is, therefore, to suppress the intergranular precipitation and promote the intragranular precipitation, having nanosized particles dispersed within the grains. This strategy not only alleviates the problem of grain boundary fracture, but also encourages dislocation trapping by the particles in the grain interior, which would help to accumulate dislocations and sustain work hardening. Nevertheless, the controlling of intragranular precipitation in UFG Al alloys is quite a challenge at present.

In this paper, we report an effective microalloying approach to boost the dispersion of precipitates in grain interior of the UFG Al alloys, and hence improve the strength/ductility combination. With trace Sc addition, we are able to achieve a predominant intragranular precipitation in UFG Al-Cu-Sc alloy, resulting in about 275% increment in ductility and simultaneously about 50% enhancement in yield strength by compared with its Sc-free counterpart where intergranular precipitation occurs even at room temperature. This microalloying approach is applicable to other UFG Al alloys and age-hardenable alloys, and paves a way for their industrial applications.

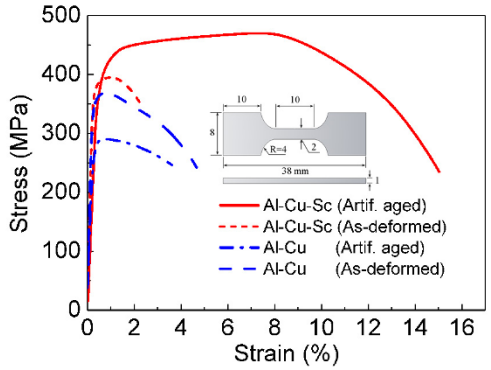

Figure 1 | Simultaneously enhanced ductility and strength in the UFG Al-Cu-Sc alloys by microalloying. Typical tensile engineering stress-strain curves of the as-processed Al-Cu-Sc (short-dash curve), Al-Cu (dash curve), and artificially aged Al-Cu-Sc (solid curve), Al-Cu (dash-dot curve) UFG alloys. The inset shows dimension of the tensile sample with a thickness of 1 mm. R is the arc indicated by the arrow. Comparison among the curves clearly indicates an improvement in ductility and simultaneously in strength after Sc addition and aging treatment.

The alloys used in this study were Al-2.5 wt% Cu (designated as Al-Cu alloys) and Al-2.5 wt% Cu-0.3 wt% Sc alloys (Al-Cu-Sc), respectively. In order to obtain UFG structures with supersaturated solid solutions, both the two alloys were immediately (within half an hour) processed by equal-channel angular pressing (ECAP) to 12 passes by route B_c after solid solution treatment. Subsequently, the samples were immediately artificially aged at 398 K for 20 h.

Results

Simultaneously enhanced ductility and strength in the UFG Al-Cu-Sc alloys by microalloying. Engineering stress-strain curves are compared in Fig. 1 between the UFG Al-Cu and Al-Cu-Sc alloys before and after artificial aging treatment, respectively. Age softening is found in the UFG Al-Cu alloy, contrary to generally observed age hardening in CG Al alloys. The as-prepared UFG Al-Cu alloy has a yield strength (σ_y) of ~365 MPa, while the aged one has a reduced σ_y of ~280 MPa, which indicates a roughly 25% drop in strength caused by aging. At the same time, the ductility of UFG Al-Cu alloy is also disappointedly reduced after aging. The total elongation to failure, ε_t, of the as-prepared UFG Al-Cu alloy can reach about 5% (dash curve), while their post-aged counterpart only has ε_t of less than 4% (dash-dot curve). On the contrary, the addition of minor Sc causes age hardening and simultaneously age ductilizing in the UFG Al-Cu alloy. The post-aged Al-Cu-Sc alloy has σ_y up to ~ 420 MPa, which is about 3.5 times of its CG Al-Cu-Sc counterpart (~ 120 MPa under the same aging treatment). Besides ~ 10% increase in σ_y, a 500% rise in ε_t is remarkably achieved in the UFG Al-Cu-Sc alloy through aging treatment (from ~ 2.5% to ~ 15.0%). The value of 15% is also 3.0 times of the tensile elongation of as-prepared UFG Al-Cu alloy. These clearly show a significant microalloying effect on mechanical properties of the UFG Al alloys.

Intergranular precipitaion in the UFG Al-Cu alloys. We will now present details of the microstructure to explain the distinct aging response between the UFG Al-Cu and Al-Cu-Sc alloys and to clarify the microalloying effect. Begin from the UFG Al-Cu alloy, Fig. 2(a) shows an electron backscatter diffraction (EBSD) orientation map of the as-prepared alloy. The average grain size was about 460 nm, and the grain boundaries were predominantly high angle grain boundaries (HAGB, $\geq 15^0$, see Supplementary Fig. S1). Besides, the average dislocation density was as high as ~ $(8.1\pm 0.3)\times10^{14}$ m^{-2}, derived from TEM measurements as well as XRD evaluations. After aged, the grains slowly grew to about 580 nm, while the dislocation density was reduced by three times, sharply down to ~ $(1.9\pm0.2)\times10^{14}$ m^{-2} (Fig. 2(b)). Three-dimensional atom probe (3DAP) element map in Fig. 2(c) showed serious Cu atom segregation at GBs. Quantitative analyses revealed that the Cu concentration at GBs (> 10%) was greater than 12 times of the nominal Cu content in the alloy(Fig. 2(d)). Careful microstructural examinations found no nanosized precipitates within the grain interior, instead numerous equilibrium θ-Al_2Cu particles (with average size ~ 45 nm) were observed at GBs, see Fig. 2(e) and (f). This meant that the precipitation in UFG Al-Cu alloys had directly gone to equilibrium θ-Al_2Cu phases and bypassed the metastable transition sequence of GP zones, θ'' and θ' as generally seen in coarse-grained Al-Cu alloys. All the θ phases had a roughly elliptical shape with their long axes in line with the grain boundary plane, indicative of the random orientation of the θ phases.

More seriously, natural precipitation of θ phases at GBs has been detected in the UFG Al-Cu alloy when stored at room temperature (RT) for longer than 10 days (Supplementary Fig. S2(a) and S2(b)). In CG Al-2.5 wt%Cu alloy, however, at least 473 K artificial aging should be required to precipitate the equilibrium θ phases directly. The notable discrepancy hints that the precipitation phase diagram of heat-treatable Al alloys has to be revised in the UFG condition (Supplementary Fig. S3). The RT decomposition and intergranular precipitation become critical problems that impact on microstructural stability of the UFG Al alloys.

Intragranular precipitaion in the UFG Al-Cu-Sc alloys. Systematical microstructure examinations proved the striking Sc microalloying effect on precipitation. The addition of minor Sc into UFG Al-Cu alloy rendered only slight variations in grain size (Fig. 3(a) and (b)), HAGBs proportion (Supplementary Fig. S1) and dislocation density (Fig. 3(b)) compared with its Sc-free counterpart (Fig. 2(a) and (b)). But the precipitation behaviors were basically changed after the Sc addition. After artificial aging, intergranular θ precipitates were seldom observed, while abundant finer θ' strengthening particles were found to be precipitated and dispersed in the grain interior (Fig. 3(e)). These θ' particles had an average size of ~ 38 nm and volume fraction up to about 1.66% (Supplementary Table S1). The θ' content in our UFG Al-Cu-Sc alloy is close to that precipitated in CG Al-Cu alloy aged at the peak aging conditions, but the θ' size is smaller than that in the aged CG alloy. These indicate that most of the excess Cu atoms have been used to form precipitates, and the Cu aggregation at GBs has been dramatically impeded. 3DAP examinations have captured the feature that the Sc atom segregation exists at the θ'/Al matrix interface (Fig. 3(c)). Previous studies have reported that the solute segregation at θ'/Al interface reduced the interfacial energy[18,19], which would slow down the growth rate of precipitates[20]. The smaller size of θ' precipitates in present UFG Al-Cu-Sc alloy is mainly ascribed to the strongly limited growth by Sc segregation at precipitate/matrix interface. Moreover, no precipitations, including intergranular θ and intragranular θ' phases, have been found in the RT-stored UFG Al-Cu-Sc alloy up to 10 days (Supplementary Fig. S2(c)), indicating a Sc-induced stabilization on RT microstructures. A threefold Sc microalloying effect in the UFG Al-Cu alloy is then ascertained, *i.e.*, retaining as-prepared microstructure at RT, reboot ing the normal precipitation sequence, and readjusting the precipi tation mode (from intergranular to intragranular one).

Discussion

Intragranular precipitation of metastable Al_2Cu phases needs the vacancy-assisted nucleation. Since the UFG materials possess a high volume of GBs than CG counterpart, depletion of vacancies is likely to occur in UFGs. As reported for Al-Cu binary alloys, artificial aging will induce a precipitate-free zone ~ 300 nm away the GB[21,22]. Therefore, it is inferred that an UFG Al-Cu alloy with grain size of ~ 600 nm will experience absorption of vacancies by the GBs

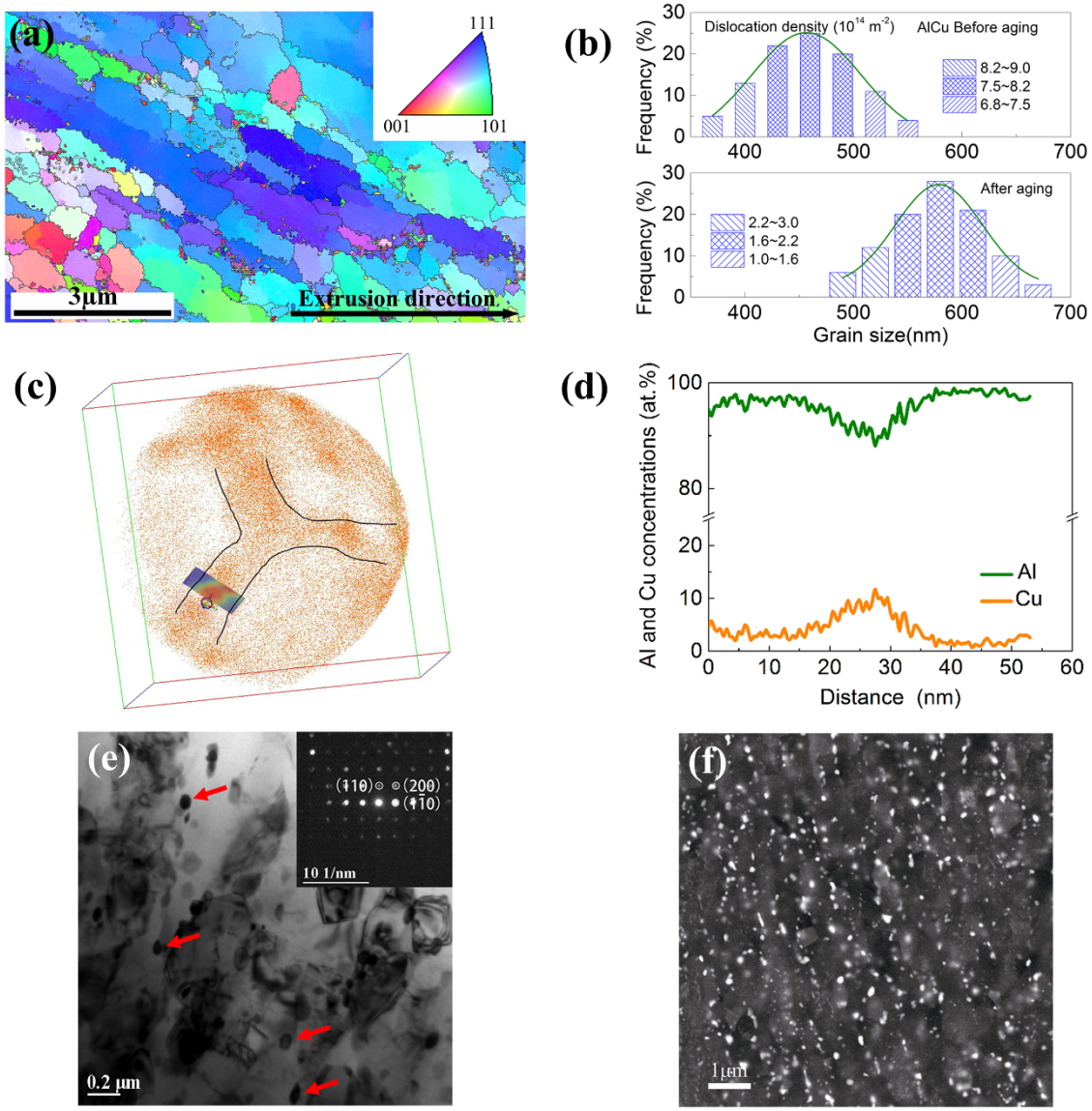

Figure 2 | Intergranular precipitaion in the UFG Al-Cu alloys. Typical microstructure of the UFG Al-Cu alloys before (a) and after (b, c, d, e, f) aging. (a) EBSD orientation maps. HAGBs (≥15°) are represented by black lines. (b) is corresponding grain size histograms, where the grain size-dependent dislocation density measured from TEM examinations is also shown and distinguished by patterns. (c) 3DAP maps showing distribution of Cu atoms naturally aged for 20 h. (orange = Cu atoms, dimensions: 40×40×30 nm). Only Cu atoms are presented in (c) for the reason of clear showing. Solid black lines in (c) display the GB regions. (d) is corresponding 1-D concentration analyses along the grain boundary marked in (c). Representative TEM, SADP (e), and BSE (f) images showing the intergranular θ-Al_2Cu precipitation after 398 K/20 h artificial aging treatment. The selected area diffraction pattern in (e) is structural analyses for the θ-Al_2Cu precipitates. Arrows in (e) and highlighted white dots in (f) typically indicate the intergranular precipitates, respectively.

on the two sides of the UFG[4,12,22]. The grains in our UFG Al-Cu alloy have an average size less than 600 nm, vacancies seem to be fully depleted within the grains, which means that nucleation of precipitates will be heavily hindered in grain interior. In the case of no intragranular precipitation, the excess Cu atoms in the supersaturated solid solute have to diffuse toward and aggregate at GBs to release the local lattice strain and reduce the system energy. This is ready to occur especially under the thermal activation and dislocation assistance. The high Cu concentration at GBs drives the nucleation and precipitation of equilibrium θ phases that need no habit requirements and therefore is energetically stable. As the intergranular particles make few contributions to strength, the strength of UFG Al-Cu alloy mainly depends on GB strengthening and dislocation strengthening. Aging treatment causes a remarkable decrease in dislocation density and a certain grain growth, both reducing the strengthening response. These are responsible for the aging softening observed in the UFG Al-Cu alloy, as show by the comparison between dash curve vs. dash-dot curve in Fig. 1. Meanwhile, the particles at GBs are prone to cause intergranular fracture, which further reduces the ductility of UFG Al-Cu alloy.

In order to stabilize the RT microstructure, suppress the intergranular precipitation and promote intragranular precipitation, we need to (i) keep most of the solute atoms and vacancies in the grain interior rather than diffuse to GBs; and (ii) promote the solute/vacancy interaction to accelerate the nucleation of intragranular particles as possible, which will exhaust the solute atoms and cut off the supply for intergranular precipitation. Sc effect on precipitation in UFG Al-Cu alloys matches well with these strategies. It has been well known that the dislocations can assist the heterogeneous nucleation of precipitates within the grains. Solute atoms are inclined to segregate near dislocation lines to release lattice distortion, forming a Cottrell atmosphere[23]. The segregation of Sc along the dislocation lines has a series

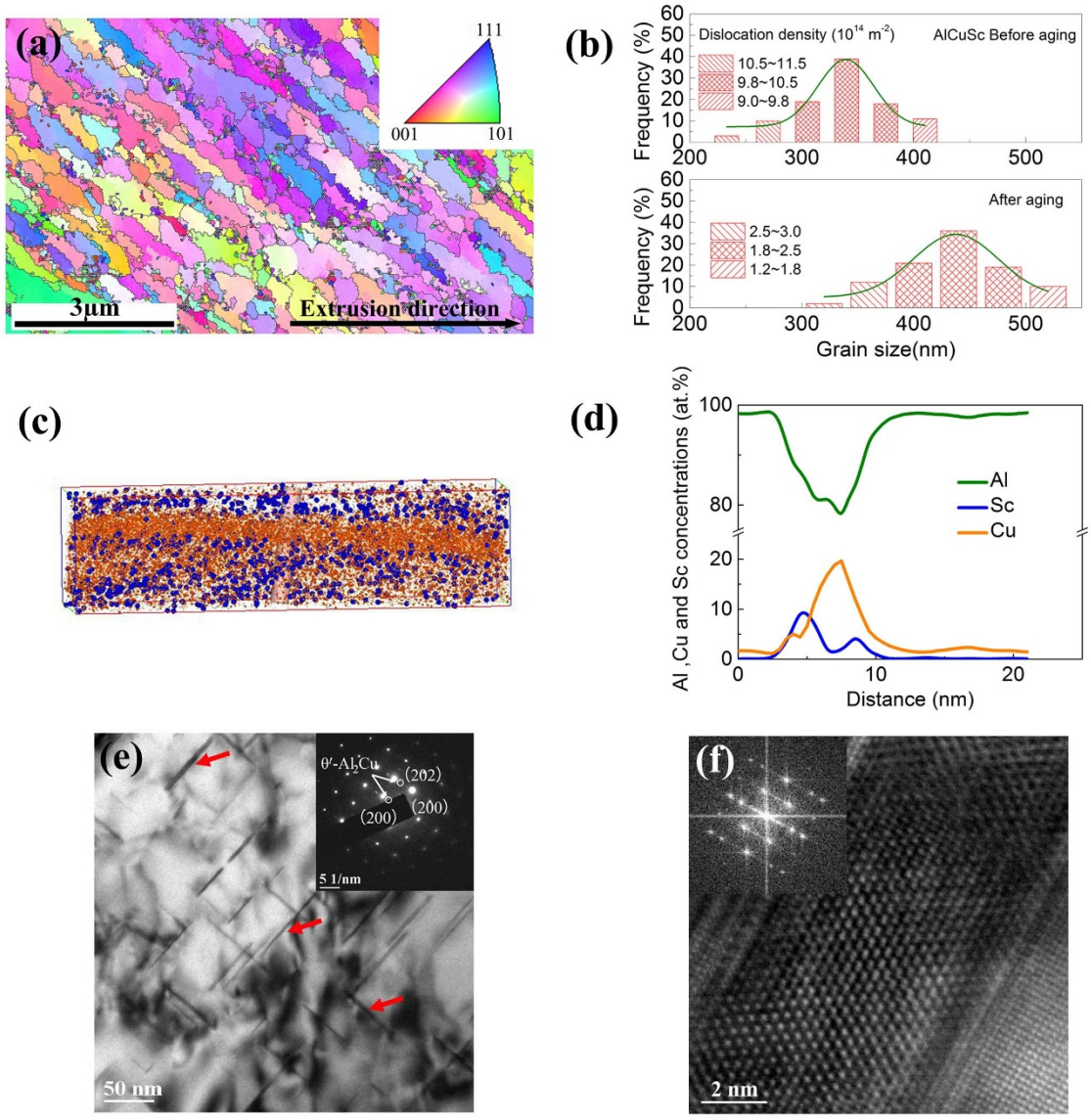

Figure 3 | Intragranular precipitaion in the UFG Al-Cu-Sc alloys. Typical microstructure of the UFG Al-Cu-Sc alloys before (a) and after (b, c, d, e, f) aging. (a) EBSD orientation maps. HAGBs (≥15°) are represented by black lines. (b) is corresponding grain size histograms, where the grain size-dependent dislocation density from TEM examinations is also shown and distinguished by patterns. (c) 3DAP maps showing distribution of Cu and Sc atoms artificially aged at 398 K for 20 h. (orange = Cu atoms, blue = Sc atoms, dimensions: 80×36×22 nm). Only Cu and Sc atoms are presented in (c) for the reason of clear showing. (d) is corresponding 1-D concentration analyses along the precipitate-matrix interface marked in (c). Representative TEM, SADP (e), and HRTEM (f) images showing the intragranular θ'-Al_2Cu precipitation after 398 K/20 h artificial aging treatment. The selected area diffraction patterns in the insert of (e) and HTREM image in (f) are structural analyses for the θ'-Al_2Cu precipitates. Arrows in (e) typically indicate the intragranular precipitates.

of advantages: Firstly, the Sc atoms are readily to trap Cu atoms because the Sc-Cu pairs are thermodynamically stable with negative enthalpy value (~ 115 kJ/mol)[24]. Because the diffusion coefficient of Sc atom in Al matrix is several orders lower than that of Cu atoms[25], the firm Sc-Cu bonding limits the diffusion of Cu atoms to the GBs. The intergranular precipitation is concomitantly repressed. Secondly, the Sc-vacancy binding energy in Al is about 0.35 eV[26], much higher than the Cu-vacancy binding energy of < 0.10 eV[27]. Therefore, the Sc atoms along the dislocation lines can also seize vacancies and stop their migration to GBs. Thirdly, the high Sc-vacancy interaction contributes to the formation of Sc-vacancy pairs which would be arranged in clusters with vacancies and multiple solute atoms. The strong Sc-Cu interaction may encourage Sc-vacancy clusters to catch Cu atoms. The Cu/Sc/vacancy complex clusters are expected to act as preferential nucleation sites for GP zones and resultantly promote the intragranular precipitation.

We now analyze the origin of the high strength and greatly enhanced ductility in the artificially aged UFG Al-Cu alloy with Sc addition. Generally speaking, these properties are borne out of the microstructures we designed and actually produced through Sc microalloying. Specifically, the high strength is expected from the UFG grains and nanoscale intragranular particles. After aging treatment, the strengthening by dispersed intragranular precipitates is predominant over the softening that is mainly caused by the decrease in dislocation density (Supplementary Table S2 and described in details in Supplementary). Ultrafine Al grains and optimized θ' strengthening particles (reduced in size and predominantly dispersed within grains) are the most important microstructural features of the aged UFG Al-Cu-Sc alloy. These refined microstructural scales impart high strength to the alloy (Supplementary Table S3). Moreover, the excellent ductility is associated with the intragranular θ' precipitates that help with the generation and storage of

dislocations (Supplementary Fig. S4 and described in details in Supplementary). In the meantime, as discussed earlier, the UFG Al-Cu-Sc microstructure also delays failure by almost fully removing the GB particles. The θ particles at GBs as observed in the aged UFG Al-Cu alloy are preferential sites for crack initiation during loading[13]. The reason is that due to deformation incompatibility, large stress concentration will be induced at the particles, inducing interfacial decohesion at the weaker GBs or particle cracking that eventually lead to microcracks along the GBs. The Sc addition, in contrast, ensures that the nanosized precipitates are mainly retained within grains. This alleviates the propensity for intergranular fracture and thus increasing the total elongation before failure. These results emphasize again that in UFG Al alloys grain boundaries should be carefully tailored in order to reach high ductility.

In summary, we have designed and successfully produced intragranular nanoparticle-dispersed UFG Al-Cu-Sc alloy, via microalloying strategy that enables the control of grains and precipitations in nanostructured regime. A high RT microstructural stability and notably enhanced tensile ductility (about tripling that of Sc-free counterpart), has been derived from the resulting UFG Al-Cu-Sc alloy. These lead us to conclude that precipitation is now controllable and tensile ductility is no longer a bottleneck for UFG Al alloys, and a similar microalloying strategy is expected to be equally effective for other UFG heat-treatable alloys such as Mg alloys and steel. Finally, the simple microalloying approach may be easily adapted to current industrial processes and hence has the potential for large-scale industrial applications.

Methods

Materials fabrication. Alloys with composition of Al-2.5 wt% Cu alloys (abbreviated Al-Cu alloys) and Al-2.5 wt% Cu-0.3 wt% Sc (Al-Cu-Sc) were respectively melted and cast in a stream argon, by using 99.99 wt % pure Al, 99.99 wt % pure Cu, and cast Al-2.0 wt% Sc alloy. No impurities were detected, considering the experimental accuracy. After homogenization treatment, billets 100 mm × Ø 10 mm were machined from the cast ingots, then solute treated in vacuum for 3 h at 853 K and immediately water-quenched to room temperature. Subsequently, the billets were immediately (within half an hour) subjected to 12 passes ECAP by route B_c[1,3], at room temperature in which the work piece was rotated 90° along its longitudinal axis in the same sense between each pass. The die for ECAP processing has an intersecting channel angle of 90° and an outer arc angle of 20°, which imposes an effective strain of approximately one per ECAP pass[1,3]. After ECAP processing, the samples were either naturally aged at room temperature (293 K) for a series of time or immediately artificially aged at 398 K for 20 h in oil bath. The maximum error of all the temperature measurements in present experiments was ± 1 K. Note that the aging treatment has been performed at different temperatures and times, but the 398 K/20 h was found to be the optimized aging parameters that resulted in the most significant microalloying effect as well as the best strength/ductility combination in the UFG Al-Cu-Sc alloy (see Supplementary Table S4).

EBSD and TEM characterazation of microstructures. Microstructures of the ECAP-processed samples were characterized by backscatter electron imaging (BSE) and electron backscattered diffraction (EBSD), which was performed on a high-resolution JSM 7001F fitted with a Pegasus XM2–EBSD system, operating at 20 kV. Specimens for SEM-EBSD observation, taken from near the center of the longitudinal transverse plane of the ECAP billets, were prepared by electro-polishing using an electrolyte of 25% nitric acid and 75% methanol at 253 K (-20°C) at an operation voltage of 15 V. To study the microstructure at nanoscale, transmission electron microscopy (TEM) was carried out by using a JEOL 2100F operating at 200 kV. Specimens for TEM analysis were prepared by twin-jet electro-polishing using the same solution. Quantitative evaluations of the number density and size of precipitates were reported as an average value of more than 600 measurements. Volume fraction of the second phase particles was determined by using corrected projection method[10]. Details about the measurements on precipitates can be referred to previous publications[10,11].

XRD characterazation of microstructures. Quantitative X-ray diffraction (XRD) measurements were performed with a Rigaku D/max-RB X-ray diffractometer, which is equipped with a Cu target and a graphite monochromator. Microstrain and dislocation density can be calculated from the XRD peak broadening, following others' work[28–30].

3DAP analysis. In order to visibly reveal the atomic distribution at atomic level, three-dimensional atom probe (3DAP) experiments were performed using an Imago Scientific Instruments 3000HR local electrode atom probe (LEAP). APT sample blanks with a square cross-sectional area of approximately 300×300 μm^2 and a 1 cm length were prepared by a combination of slicing and mechanical grinding. A two-step electropolishing procedure was used for making tips from these blanks[31,32]. A 10 vol.% perchloric acid in methanol solution was used for coarse polishing, and the final polishing was performed using a solution of 2 vol.% perchloric acid in butoxyethanol. APT data collection using the electrical pulsing mode was performed at a specimen temperature of 30±0.3 K, with a voltage pulse fraction (pulse voltage/steady-state DC voltage) of 20%, a pulse repetition rate of 200 kHz and a background gauge pressure of $< 6.7\times10^{-8}$ Pa (5×10^{-10} torr).

Mechanical response test. Tensile testing was used to measure yield strength and ductility (elongation to failure) of the samples before and after artificial aging treatment. Smooth tensile specimens have a gauge size of 1 *mm* in thickness, 2 *mm* in width, and 10 *mm* in length, with axis along the extrusion direction. The testing was performed using a MTS-C43Tester at a constant strain rate of 2×10^{-4} s^{-1} with the load direction parallel to the specimen axis. Engineering stress-strain curves were automatically recorded and the yield strength was determined as the 0.2% offset.

1. Valiev, R. Z., Islamgaliev, R. K. & Alexandrov, I. V. Bulk nanostructured materials from severe plastic deformation. *Prog. Mater. Sci.* **45**, 103–189 (2000).
2. Zhilyaev, A. P. & Langdon, T. G. Using high-pressure torsion for metal processing: Fundamentals and applications. *Prog. Mater. Sci.* **53**, 893–979 (2008).
3. Sabirov, I., Murashkin, M. Y. & Valiev, R. Z. Nanostructured aluminium alloys produced by severe plastic deformation: New horizons in development. *Mat. Sci. Eng. A* **560**, 1–24 (2013).
4. Sauvage, X., Wilde, G., Divinski, S. V., Horita, Z. & Valiev, R. Z. Grain boundaries in ultrafine grained materials processed by severe plastic deformation and related phenomena. *Mat. Sci. Eng. A* **540**, 1–12 (2012).
5. Ma, E. Eight routes to improve the tensile ductility of bulk nanostructured metals and alloys. *Jom* **58**, 49–53 (2006).
6. Liddicoat, P. V. *et al.* Nanostructural hierarchy increases the strength of aluminium alloys. *Nat Commun* **1**, 63 (2010).
7. Han, B. Q., Huang, J. Y., Zhu, Y. T. & Lavernia, E. J. Strain rate dependence of properties of cryomilled bimodal 5083 Al alloys. *Acta Mater.* **54**, 3015–3024 (2006).
8. Zhao, Y.-H., Liao, X.-Z., Cheng, S., Ma, E. & Zhu, Y. T. Simultaneously increasing the ductility and strength of nanostructured alloys. *Adv. Mater.* **18**, 2280–2283 (2006).
9. Horita, Z., Ohashi, K., Fujita, T., Kaneko, K. & Langdon, T. G. Achieving High Strength and High Ductility in Precipitation-Hardened Alloys. *Adv. Mater.* **17**, 1599–1602 (2005).
10. Liu, G., Zhang, G. J., Ding, X. D., Sun, J. & Chen, K. H. Modeling the strengthening response to aging process of heat-treatable aluminum alloys containing plate/disc- or rod/needle-shaped precipitates. *Mat. Sci. Eng. A* **344**, 113–124 (2003).
11. Liu, G. *et al.* Heat treatment-modulated coupling effect of multi-scale second-phase particles on the ductile fracture of aged aluminum alloys. *Acta Mater.* **55**, 273–284 (2007).
12. Huang, Y., Robson, J. D. & Prangnell, P. B. The formation of nanograin structures and accelerated room-temperature theta precipitation in a severely deformed Al–4 wt.% Cu alloy. *Acta Mater.* **58**, 1643–1657 (2010).
13. Liu, G. *et al.* Nanostructured high-strength molybdenum alloys with unprecedented tensile ductility. *Nat. Mater.* **12**, 344–350 (2013).
14. Kim, J. K., Kim, H. K., Park, J. W. & Kim, W. J. Large enhancement in mechanical properties of the 6061 Al alloys after a single pressing by ECAP. *Scripta Mater.* **53**, 1207–1211 (2005).
15. Hockauf, M. *et al.* Simultaneous improvement of strength and ductility of Al–Mg–Si alloys by combining equal-channel angular extrusion with subsequent high-temperature short-time aging. *Mat. Sci. Eng. A* **503**, 167–171 (2009).
16. Hockauf, K., Meyer, L. W., Hockauf, M. & Halle, T. Improvement of strength and ductility for a 6056 aluminum alloy achieved by a combination of equal-channel angular pressing and aging treatment. *J. Mater. Sci.* **45**, 4754–4760 (2010).
17. Kim, W. J., Chung, C. S., Ma, D. S., Hong, S. I. & Kim, H. K. Optimization of strength and ductility of 2024 Al by equal channel angular pressing (ECAP) and post-ECAP aging. *Scripta Mater.* **49**, 333–338 (2003).
18. Biswas, A., Siegel, D. J. & Seidman, D. N. Simultaneous Segregation at Coherent and Semicoherent Heterophase Interfaces. *Phys. Rev. Lett.* **105**, 076102 (2010).
19. Biswas, A., Siegel, D. J., Wolverton, C. & Seidman, D. N. Precipitates in Al–Cu alloys revisited: Atom-probe tomographic experiments and first-principles calculations of compositional evolution and interfacial segregation. *Acta Mater.* **59**, 6187–6204 (2011).
20. Kirchheim, R. Grain coarsening inhibited by solute segregation. *Acta Mater.* **50**, 413–419 (2002).
21. Hirosawa, S., Oguri, Y. & Sato, T. Experimental and computational investigation of formation of precipitate free zones in an Al-Cu alloy. *Mater. Trans.* **46**, 1230 (2005).
22. Hu, T., Ma, K., Topping, T. D., Schoenung, J. M. & Lavernia, E. J. Precipitation phenomena in an ultrafine-grained Al alloy. *Acta Mater.* **61**, 2163–2178 (2013).
23. Blavette, D., Cadel, E., Fraczkiewicz, A. & Menand, A. Three-Dimensional Atomic-Scale Imaging of Impurity Segregation to Line Defects. *Science* **286**, 2317–2319 (1999).
24. Niessen, A. K. *et al.* Model predictions for the enthalpy of formation of transition metal alloys II. *Calphad.* **7**, 51–70 (1983).

25. Chen, B. A. *et al.* Effect of interfacial solute segregation on ductile fracture of Al–Cu–Sc alloys. *Acta Mater.* **61**, 1676–1690 (2013).
26. Miura, Y., Joh, C. H. & Katsube, T. Determination of vacancy-Sc interaction energy by electrical resistivity measurements. *Mater. Sci. Forum* **331–337**, 1031–1035 (2000).
27. Wolverton, C. Solute-vacancy binding in aluminum. *Acta Mater.* **55**, 5867–5872 (2007).
28. Williamson, G. K. & Smallman, R. E. III. Dislocation densities in some annealed and cold-worked metals from measurements on the X-ray debye-scherrer spectrum. *Philosophical Magazine* **1**, 34–46 (1956).
29. Zhao, Y. H., Liao, X. Z., Jin, Z., Valiev, R. Z. & Zhu, Y. T. Microstructures and mechanical properties of ultrafine grained 7075 Al alloy processed by ECAP and their evolutions during annealing. *Acta Mater.* **52**, 4589–4599 (2004).
30. Gubicza, J. *et al.* The effect of severe plastic deformation on precipitation in supersaturated Al–Zn–Mg alloys. *Mat. Sci. Eng. A* **460–461**, 77–85 (2007).
31. Krakauer, B. W. & Seidman, D. N. Systematic procedures for atom-probe field-ion microscopy studies of grain boundary segregation. *Rev. Sci. Instrum.* **63**, 4071–4079 (1992).
32. Miller, M. K. Atom Probe Tomography: Analysis at The Atomic Level. (Kluwer Academic/Plenum Publishers, New York, 2000).

Acknowledgments

This work was supported by the National Natural Science Foundation (51321003, 51322104, 51171142 & 51201133), the National Basic Research Program of China (973 program, Grant No. 2010CB631003 & 2012CB619600), and the 111 Project of China (B06025). GL thanks the financial support of Fundamental Research Funds for the Central Universities and TengFei Scholar project. RHW thanks the support of Natural Science Foundation of ShaanXi Province of China (2010JK758).

Author contributions

J.S. and G.L. designed and supervised the project, L.J., J.K.L., P.M.C., R.H.W., B.A.C., J.Y.Z., M.X.Y. and G.Y. carried out the experiments, L.J., P.M.C. and G.L. performed the calculations, L.J. and G.L. wrote the paper. All the co-authors contribute to discussions.

Additional information

Supplementary information accompanies this paper at http://www.nature.com/scientificreports

Competing financial interests: The authors declare no competing financial interests.

How to cite this article: Jiang, L. *et al.* Microalloying Ultrafine Grained Al Alloys with Enhanced Ductility. *Sci. Rep.* **4**, 3605; DOI:10.1038/srep03605 (2014).